Numerical study of the blockage length effect on the transient wave in pipe flows

MING ZHAO, Associate Professor, *Department of Engineering Mechanics, Dalian University of Technology, Dalian, People's Republic of China*

Email: zhaoming@dlut.edu.cn (author for correspondence)

MOHAMED S. GHIDAOUI (IAHR Member), Chair Professor, *Department of Civil and Environmental Engineering, Hong Kong University of Science and Technology, Hong Kong SAR, People's Republic of China*

Email: ghidaoui@ust.hk

MOEZ LOUATI (IAHR Member), Post-doctoral Fellow, *Department of Civil and Environmental Engineering, Hong Kong University of Science and Technology, Hong Kong SAR, People's Republic of China*

Email: mlouati@ust.hk

HUAN-FENG DUAN (IAHR Member), Assistant Professor, *Department of Civil and Environmental Engineering, Hong Kong Polytechnic University, Hong Kong SAR, People's Republic of China*

Email: hf.duan@polyu.edu.hk

Running Head: Pipe transient and extended blockage

Numerical study of the blockage-length effect on transient waves in pipe flows

ABSTRACT

A pipeline with an extended blockage is modelled as a system of three pipes in series. A computational fluid dynamics approach using the ADINA software is adapted to solve the slightly compressible turbulent flow problem with complex geometry. Two-dimensional axisymmetric computational results are validated by several examples. In practice, the water hammer wave generated by rapid valve closure usually exhibits wave front smearing. The numerical analysis shows that for a blockage length larger than the wave front thickness, the magnitude of the incident wave may be significantly suppressed as a result of the interaction between the blockage and the wave front. By reflecting negative pressure waves toward the incident wave before its maximum pressure arrives at the blockage, the maximum transient pressure may be considerably reduced. Consequently, the blockage behaves as a discrete blockage. However, if the blockage length is large compared with the thickness of the wave front, the incident wave conserves its initial amplitude, and the blockage behaves as an extended blockage. Therefore, the occurrences of discrete and extended blockages depend on the thickness of the wave front and thus on the rapidity of the maneuver that generates the transient.

Keywords: Blockage; computational fluid dynamics; numerical diffusion; transient; water pipeline; wave

1 Introduction

Blockages exist in many pipeline systems and cause problems. A blockage in a cardiovascular system due to the plaque deposits leads to possible heart attack problems (Quarteroni, 2001). A delay in finding the real blockage in a district heating system causes thousands of people to be “homeless” for several days in a frozen winter (Jiang, Chen, & Li, 1996). Partial blockage in natural gas transportation pipeline causes loss of deliverability and higher compression costs (Adewumi, Eltohami, & Ahmed, 2000; Adewumi, Eltohami, & Solaja, 2003). The blockage in water transport pipeline also leads to lower delivery efficiency and sometimes even causes safety problems (Wang, Lambert, & Simpson, 2005).

Locating blockages and estimating their dimensions in a timely manner are important in order to minimize damage to pipes and pumping equipment as well as to reduce product and energy losses in pipeline systems. Various approaches have been developed to detect blockages in ducts. When a blockage is at the end of a duct, Wu & Fricke (1989) use acoustic eigenfrequency shifts to estimate the dimension of partial blockage. De Salis & Oldham (1999, 2001) consider eigenfrequency shifts together with anti-resonance value shift, and are able to re-construct the area profile of a duct with one open boundary. Jiang et al. (1996)

monitor the pressure change in a district heating system and are able to locate a blockage according to the whole system relation between the blockage and pressure changes. Wang et al. (2005) use damping of pressure transients to locate the blockage for a single pipe line system. Mohapatra, Chaudhry, Kassem, & Moloo (2006) introduce steady oscillation flow in a pipe system and investigate the peak pressure frequency response at the valve to detect partial blockage in a single pipeline. The pressure peak is associated with odd harmonics. Sattar, Chaudhry, & Kassem (2008) use a similar approach with even harmonics to detect partial blockage. Lee, Vítkovský, Lambert, Simpson, & Liggett (2008) find that discrete blockages induce an oscillatory pattern in the peak frequency response diagram, which can be related to the location and size of the blockage.

Frequency response-based techniques (e.g., Lee, Duan, Ghidaoui, & Karney, 2013; Lee et al., 2008; Mohapatra et al., 2006; Sattar et al., 2008) are applicable for locating and sizing blockages provided that the blockage can be approximated as a localized discontinuity in the system. However, most blockages from pipe deterioration occur over significant pipe lengths. Brunone, Ferrante, & Meniconi (2008) show that discrete and extended blockages have significantly different impacts on the system responses; thus, techniques for discrete blockages may not be applicable for extended blockage situations. Duan, Lee, Ghidaoui, & Tung (2012) investigate the behavior of blockages in a pipeline under transient conditions and develop an analytical expression of the frequency response of a pipeline partially blocked by an arbitrary number of internal extended blockages. The derived analytical solutions are further examined and validated numerically in Duan, Lee, Ghidaoui, & Tuck (2014). Thereafter, an extended study by Duan (2016) examines systematically the sensitivity of the frequency response-based methods to different influence factors in water pipeline systems. These works have also identified a critical need for understanding wave scattering from defects.

The laboratory experiments (Contractor, 1965; Duan et al., 2017; Duan et al., 2013; Meniconi, Brunone, & Ferrante, 2011, 2012; Meniconi, Brunone, Ferrante, & Massari, 2011, 2012) are additional key studies that point to a need for understanding wave-defect interaction in pressurized systems if blockages are to be successfully located and their sizes predicted. Such experiments reveal that wave-defect interaction leads to unexplained and complicated flow behavior such as the apparent independence of the reflected wave to the amplitude of the incident wave; the stark asymmetry between the first half of the wave cycle and the second half of the wave cycle; and the appearance of isolated pressure “mounds” in the case of defects that cause near full-pipe blockage. Clearly, the flow separation due to the sudden contraction and expansion of the pipe at the defect, and its interaction with the incident as well the waves that are subsequently reflected from various hydraulic elements, plays a central role in the flow dynamics.

Laboratory experiments capable of in-depth examination of wave and defect interaction are highly challenging given the high frequency of water hammer waves, the large disparity between the wave and turbulence time scales, and the difficulty in designing excitation strategies that are repeatable so that ensemble averaging is possible. As an alternative, results generated from a validated numerical model are, in some cases, helpful to the study of detailed flow fields.

The three-dimensional turbulent nature of the flow field in the vicinity of a defect, together with the fact that the flow is slightly compressible, suggests that that a three-dimensional turbulent transient wave model is needed to correctly predict the nature of the flow field. The governing equations in such a model are the three-dimensional Navier-Stokes equations for compressible low Mach number flows. The wave speed relation includes the effect of water compressibility and pipe/soil elasticity. The problem also involves the interaction of strong turbulence and sharp waves. However, there is currently no numerical model that incorporates all these features. As an alternative approach, the local energy loss due to a blockage can be approximated by using an axisymmetric model as an initial approximation. The intrinsic three dimensionality of turbulence can also be approximated by a Reynolds averaged Navier-Stokes equation (RANS) approach, such as two-equation turbulence models. Along this line, Mitra & Rouleau (1985) built a two-dimensional model for transient pipe flow. Vardy & Hwang (1991) neglected pressure variation in the radial direction and considered a plane wave solution with an algebraic turbulence model. Zhao & Ghidaoui (2003) modified Vardy and Hwang's numerical scheme and built an efficient quasi-two-dimensional model. The quasi-two-dimensional model is capable of accounting for the velocity profile and dissipation due to viscosity for pipe without partial blockage. However, the quasi-two-dimensional model is not able to simulate pipes with partial blockages as the flow field is such that it minimally requires true two-dimensionality with the radial velocity component being taken into account. A possibility for developing such a model is to extend the model of Mitra & Rouleau (1985) to more complicated geometry. Alternatively, a general purpose computational fluid dynamics (CFD) software package may be employed as this class of model is capable of handling complex geometry. Since the goal of the present study focuses on the interaction between local defect and transient pressure waves, the latter approach is adopted in the present work.

Many third-party commercial software packages for CFD are readily available, including Fluent, CFX, Flow-3D, and many others. For the current water hammer case, where the fluid is considered slightly compressible, the commercial software ADINA is well suitable. ADINA R&D, Inc. was founded in 1986 by Dr. K. J. Bathe and Associates. The ADINA System is used for linear and nonlinear finite element analysis of solids and structures, heat transfer, fluids and electromagnetics. ADINA also offers a comprehensive

array of multi-physics capabilities, including fluid-structure interaction and thermo-mechanical coupling. In this paper, the pipe wall is considered to be rigid and only the fluid flow is studied. In the near future, pipe wall elasticity or pipe wall viscoelasticity will be studied in situations where fluid-structure interaction is considered to be important.

2 Introduction

In ADINA, the slightly compressible flow state equation is (ADINA modeling guide):

$$\rho_m = \rho(1+\frac{p}{K}) = \rho + \frac{p}{a_0^2} \tag{1}$$

where ρ_m is the fluid density with the compressibility, ρ is the density at zero pressure $p = 0$, K is the bulk modulus of elasticity of fluid, and a_0 is the wave speed. Therefore, the continuity equation is:

$$\frac{\rho}{K}\left(\frac{\partial p}{\partial t} + \boldsymbol{v} \bullet \nabla p\right) + \rho_m \nabla \bullet \boldsymbol{v} = 0 \tag{2}$$

where $\boldsymbol{v}$ is the velocity vector, t is the time. The equations for motions are:

$$\left(\rho + \frac{p}{a_0^2}\right)\frac{\partial \boldsymbol{v}}{\partial t} + \rho \boldsymbol{v} \bullet \nabla \boldsymbol{v} - \nabla \bullet \boldsymbol{\tau} = \boldsymbol{f}^B \tag{3}$$

where $\boldsymbol{\tau}$ is the stress tensor, $\boldsymbol{f}^B$ is the body force vector. For laminar flow case, the stress tensor is:

$$\boldsymbol{\tau} = \left(-p + \lambda \nabla \bullet \boldsymbol{v}\right)\mathbf{I} + \mu\left(\nabla \boldsymbol{v} + \nabla \boldsymbol{v}^T\right) \tag{4}$$

where μ and λ are the two coefficients of fluid viscosity and $\mathbf{I}$ is the unit tensor. For turbulent flows, a *k-e* model with wall function is used to evaluate the turbulent viscosity μ_t to replace the fluid viscosity μ in this paper.

Note that p is of order $\rho a_0 V$, where V is the velocity scale. As a result, the multiplier of the temporal acceleration in equation (3) is of order $\rho(1+V/a_0)$. For water hammer application, V/a_0 is typically of order 1/1000; thus, $\rho(1+V/a_0) \approx \rho$, equation (3) becomes:

$$\rho\frac{\partial \boldsymbol{v}}{\partial t} + \rho \boldsymbol{v} \bullet \nabla \boldsymbol{v} - \nabla \bullet \boldsymbol{\tau} = \boldsymbol{f}^B \tag{5}$$

A finite element method is used to solve the continuity and momentum equations. For fluid elements, flow-condition based interpolation functions are used, and the order of accuracy for spatial discretization can be first or second order. First or second order of accuracy implicit

time-integration is used. Although ADINA is a general purpose CFD package and has the ability to solve flows in an arbitrary three-dimensional domain, it is computationally time consuming when a three-dimensional problem is solved. In the current study, only the axisymmetric flow problem is simulated to reduce the computational burden.

3 Results

3.1 Model validation

To validate the computational results from the ADINA software, the following scenarios are considered.

Case 1: The first scenario involves a stoppage of a steady state pipe flow by a sudden valve closure which was simulated by Mitra & Rouleau (1985). The flow parameters are $R =$ pipe radius = 0.0127m, $V_0 =$ steady state mean velocity = 0.156m s^{-1}, density $\rho =$ 876.144kg m^{-3}, dynamic viscosity $\mu = 3.48 \times 10^{-2}$ kg m^{-1}s^{-1} and bulk modulus of elasticity $K = 1.54 \times 10^{9}$ Pa. The valve closure time is 3.84×10^{-6} s. For comparison, the spatial and temporal grid sizes are the same as those used in Mitra & Rouleau (1985), i.e., $\Delta x = \Delta r = 0.05R = 6.35 \times 10^{-4}$ m , where x is the axial coordinates, r is the radial coordinate, $\Delta t = 0.05R / a_0 = 4.8 \times 10^{-7}$ s . The Reynolds number in this case is $\mathrm{R} = 100$ thus the steady state flow is laminar.

Pressure signals at the valve at different radial locations are plotted in Fig. 1. The computational results from ADINA generally agree with the numerical results from Mitra & Rouleau (1985). The relative pressure surge at $r/R = 0$ is close to 2, which is about twice as large as the Joukowsky pressure. The reason is that the maximum velocity at the centerline is twice the average velocity for a steady state pipe Poiseuille flow. Therefore, valve closure arrests a fluid whose velocity at the center is twice the cross sectional average velocity. However, the pressure settles fairly quickly back to the Joukowsky pressure after 7 to 8 R/a_0, where R/a_0 is travel time of the wave in the radial direction from the pipe centerline to the pipe wall. This test case, and the comparison with previously published results, provides support for the use of ADINA in modeling two-dimensional (axisymmetric) water hammer waves in pipes.

Case 2: The second scenario investigates the ability of ADINA to model a transient wave generated by pressure pulse at the downstream end of the pipe, where the shape of the pulse is identical to that in Mitra & Rouleau (1985). In this case, $\rho =$ 789.045 kg m^{-3}, $R = 7.62$ mm, the pressure pulse amplitude is $p = 0.6895$ MPa, $\mu = 3.23 \times 10^{-3}$ kg m^{-1}s^{-1},

$K = 1.43 \times 10^9$ Pa. All other parameters, including spatial and temporal step size ratios ($\Delta x = \Delta r = 0.05R$, $\Delta t = 0.05R / a_0$), are the same as in case 1. The temporal variation in pressure at different stations along the pipe axis is plotted in Fig. 2, where x/R corresponds to the pressure pulse location. Again, the computational results from ADINA generally agree with the numerical results from Mitra & Rouleau (1985). When the pressure pulse propagates along the pipeline (say, at $x/R = 1.0, 2.0, 3.0$), its sharp and square wave shape becomes smoothed with time due to numerical diffusion of the implicit scheme used. This is illustrated in Figs 2 and 3.

Pressure traces for different time step sizes and different orders of accuracy of time integration schemes are plotted in Fig. 3. Decreasing the time step duration for first order time integration, for example when the time step size is changed from $\Delta t = 2.83 \times 10^{-7}$s to $\Delta t = 0.707 \times 10^{-7}$s, the numerical diffusion is reduced. For the original (larger) time step ($\Delta t = 2.83 \times 10^{-7}$s) the second order time integration scheme produces much less numerical diffusion, however, severe post-shock oscillations arise and these numerical aberrations are undesirable. The above results are obtained for spatial grid size $\Delta x = \Delta r = 0.381$ mm, which is used in Mitra & Rouleau (1985). When the time step $\Delta t = 2.83 \times 10^{-7}$s is fixed, calculation shows that, for different spatial grid sizes, the solution converges to the case with $\Delta x = 0.0953$ mm and $\Delta r = 0.0476$ mm. These results show that the numerical diffusion depends on the grid sizes both in time and space. However, the numerical diffusion is necessary in this case for obtaining a stable solution as a very strong discontinuity exists in the current scenario due to the nearly instantaneous pulse generation of the initial transient pressure wave. Naturally, accuracy and stability of the solution depend on grid size and this should be considered when applying the numerical model to other pipe transient problems.

Case 3: The third scenario is designed to test the validity of the turbulence model in ADINA. For this purpose, a turbulent steady state flow is used so that the model velocity profile can be compared with the log-law velocity profile. The steady, cross-sectional mean flow velocity is 1m s^{-1}, the pipe diameter is 0.1m, and the fluid viscosity is 10^{-6} m^2s^{-1}. The Reynolds number is $\mathrm{R} = 10^5$. The corresponding friction factor for smooth pipe obtained from the Moody diagram is 0.0176 (Street, Watters, & Vennard, 1996). In ADINA, a two-layer turbulence model is adopted where the whole domain is subdivided into a near-wall viscous region and a fully turbulent region. The friction factor calculated by ADINA is 0.0181. The friction factor calculated by a low-Reynolds number k-epsilon model (Zhao & Ghidaoui, 2006) is 0.0179. The friction factor predicted by ADINA is about 3% higher can considered to be in good agreement with the empirical value. The normalized profile of time-averaged velocity in terms of wall coordinates (u^+, y^+) is plotted in Fig. 4. The results for

different radial discretization (Nr is defined as the number of grid steps in the radial direction) are considered to have converged to very similar solution results.

3.2 Model validation

A reservoir-pipe-valve system with an extended blockage (Fig. 5) is considered. The total length of the original unblocked pipe is $L = 100$ m, its diameter $D =$ 0.1 m, and the steady state water velocity in it is $V_0 = 1$m s^{-1}. The bulk modulus of elasticity is 2.0 GPa and fluid density is 1000 kg m^{-3}. The flow is turbulent (Reynolds number 10^5). The upstream constant pressure head is specified as 204.08m ($p = 2.0$MPa). The blockage is modeled as a pipe section with smaller diameter $d = 0.04$ m and length $l = 10$ m. The blockage starts at 55m from the upstream reservoir. Thus, the original pipe is effectively made up of three pipes in series with lengths 55 m, 10 m and 35 m, respectively.

The steady state energy grade line calculated from ADINA is plotted for different axial grid resolutions in Fig. 6. The slope of the energy grade line due to friction loss is almost the same for different grid size implying that numerical dissipation is minimal. However, the minor loss (i.e., loss due to flow separation at the junction) depends on the grid size as can be seen from the large difference between the results for $\Delta x = 0.2$ m and $\Delta x = 0.1$ m. However, the difference between the results progressively diminishes as the step size is refined. In fact, the minor losses for $\Delta x = 0.02$ m and $\Delta x = 0.05$ m are very close, indicating numerical convergence. According to the empirical formula in Street, Watters, & Vennard (1996), the minor losses at station 55 m and 65m are 0.86 m and 1.40 m, respectively. ADINA model results give 0.8 m and 1.7 m, respectively.

A transient pressure wave is induced by sudden closure of the downstream valve at $t = 10$ s. The pipe is considered rigid; thus, the wave speed is $a_0 = \sqrt{K/\rho} = 1414$ m s^{-1}, which gives a Joukowsky water hammer pressure $H_0 = a_0 V_0 / g = 144.3$ m, where $g = 9.81$ m s^{-2} is the gravitational acceleration constant. The pressure head traces for different grid refinements at the valve end are plotted in Fig. 7. The noticeable difference in the pre-transient pressure, especially for the case $\Delta x = 0.2$ m, is due to the errors in the steady state pressure induced by inaccurate calculation of minor losses when the grid is not fine enough (as was discussed in the previous paragraph and shown in Fig. 6).

A detailed plot of pressure traces for shorter duration is shown in Fig. 8. The spatial grid is $\Delta x = 0.02$ m. The results also show that numerical diffusion is reduced as the time discretization is refined. In Fig. 8, point A corresponds to the time just before the valve closure. Point B corresponds to the time slightly after valve closure. Thus, the pressure jump from A to B represents the magnitude of the wave that will be incident at the blockage. Point

C corresponds to the time when the first reflected wave (from blockage right end) returns to the valve from the blockage location. Therefore, the pressure at C is the sum of the incident wave plus the magnitude of the wave reflected back towards the valve from the incident wave at the right end of the blockage. A portion of the incident wave is transmitted through the blockage region. As this transmitted portion of the wave reaches the left side of the blockage, the rapid expansion of the pipe diameter acts similarly to a reservoir and a negative wave reflection occurs at the junction of the blockage and the pipe connecting the blockage to the reservoir. Point D corresponds to the time when this second (negative) reflected wave (from blockage left end) returns to the valve. ADINA gives $H_A = 192.4\,\text{m}, H_B = 338.2\,\text{m}$ and thus $(H_B - H_A)/H_0 = 1.01$. Note the results are obtained with a two-dimensional turbulent flow model. As this is a highly turbulent flow the steady state velocity distribution is almost uniform with respect to the radial coordinate. Therefore, the pressure jump due to sudden valve closure $(H_B - H_A)$ is very close to the theoretical Joukowsky pressure (H_0). The Joukowsky water hammer pressure calculated by ADINA is 1% different from the theoretical value.

The pressures at C and D involve a series of complex wave transmissions and reflections. The analysis of these pressures sheds light on the accuracy of ADINA at investigating wave transmission and reflection from blockages and other discontinuities in the system. With this in mind, ADINA computes $H_C = 549.4\,\text{m}$, $H_D = 452.9\,\text{m}$, or $(H_C - H_A)/H_0 = 2.474$, $(H_D - H_A)/H_0 = 1.805$. According to the method of characteristics (MOC) solution (Wylie, Streeter, & Suo, 1993), which is used to study wave transmission and reflection at junctions of pipe in series, when a transient wave of amplitude ($H_W - H_A$) arrives at a pipe junction, the reflected wave $H_j - H_A$ obeys the relation $(H_j - H_A)/(H_W - H_A) = 2/(1 + A_1/A_2)$, where A_1 and A_2 represent pipe cross sectional areas downstream and upstream of junction relative to incident wave, respectively. In the current valve-pipe-blockage-pipe case (Fig. 5), when the wave generated by the valve closure impinges on the blockage, its amplitude gets multiplied by a factor of $2/(1+0.04^2/0.1^2) = 1.724$. Therefore, the reflected and transmitted wave amplitude at the blockage is $H - H_A = 1.01H_0 \times 1.724 = 1.741H_0$, which is $1.741H_0 - 1.01H_0 = 0.73H_0$ greater than the incident wave (called "wave focusing). When this reflected wave impinges on the valve its amplitude becomes $0.73H_0 \times 2 + 1.01H_0 = 2.473H_0$. This result is in good agreement with ADINA which gives $H_C - H_A = 2.474H_0$. For the pressure at D, the calculation is more involved, but can be done.

As was shown in the previous paragraph, when the wave due to the valve closure travels into the blockage, the transmitted wave is $H - H_A = 1.741H_0$. This wave travels further upstream and upon arriving at the upstream end of the blockage it gets reflected again. When the wave in the blockage impinges on the normal pipe the amplitude gets multiplied by a factor $2/(1+0.1^2/0.04^2) = 0.276$, therefore the reflected amplitude is $1.741H_0 \times 0.276 = 0.480H_0$, which is $0.480H_0 - 1.741H_0 = -1.261H_0$ smaller than the incident wave. This reflected wave whose amplitude is $-1.261H_0$ propagates towards the right side of the blockage (see Fig. 5). The transmitted wave from the right hand side of the blockage towards the valve is $-1.261H_0 \times 0.276 = -0.348H_0$. Therefore, the total pressure at the valve is $-0.348H_0 \times 2 + 2.473H_0 = 1.777H_0$, which is close to that obtained from the ADINA software, $(H_D - H_A)/H_0 = 1.805$. Thus, ADINA can capture the complicated wave reflection and transmission processes in the series pipelines. Figure 8 also shows that as far as the typical points, i.e., A, B, C, D are concerned, the pressure heads converge for different time steps, and the numerical diffusion in this case will not change the results.

The blockage length is then shrunk to zero, that is, point 1 and 2 become coincident in Fig. 5 as are points 3 and 4. The spatial grid size at the two sides of the blockage along the pipe is 0.02 m. This blockage case is adopted to mimic a discrete blockage. To induce sufficient local (minor) head loss at the blockage, the inner diameter of the blocked plate is reduced to 0.026m. The local energy loss is primarily due to flow separation at the right side of the pipe junction (Fig. 5). The blockage is located at 60m from the reservoir. The downstream valve is suddenly closed at $t = 10$ s and the resulting pressure signal at the valve is plotted in Fig. 9.

The initial pressure at point A is the steady state pressure and the pressure at point B is the sum of the steady state pressure and the Joukowsky transient pressure. It is common to represent local energy losses as a discrete blockage (loss) through the introduction of a so-called minor loss relation. In fact, the energy loss can be a significant portion of the total pressure head although it is a local or “discrete” phenomenon in relation to the total length of the pipe system. Generally, the terms discrete or local loss are preferred although the traditional terminology of minor loss remains copiously in the literature (Contractor, 1965; Meniconi, Brunone, & Ferrante, 2011). It is easy to obtain that the total energy loss in the current system at steady state is 30.5 m. In one dimensional model, this minor loss, being a function of velocity, is annihilated during an instantaneous valve closure when the maximum pressure pulse reduces the flow velocity to zero; thus, the pressure head at C is expected to be 30.5 m higher than that at location B. It is instructive to note that the two-dimensional results of ADINA give $H_C - H_B = 29.9$ m (Fig. 9), which is only 2% different from the result

obtained by the minor loss calculation. Therefore, ADINA represents the flow separation well in terms of correctly predicting the local energy loss.

Overall, the above results show that ADINA models well the physics of the complicated wave patterns, skin friction and form drag taking place in blocked pipes and/or in a system with pipes in series. Therefore, ADINA is used in the remainder of this paper to examine some aspects of the interaction between transient waves and blockage.

3.3 Flow field around the blockage

The velocity vector at the blockage at different times is plotted in Fig. 10. The results shown in the figure are for a 1m long blockage. At $t =$ 10 s, the transient pressure wave is generated at the valve end, and the velocity in the blockage section is the steady state velocity profile. The flow separation at the downstream end of the blockage is evident in the figure. At $t = 10.027$s, the wave front arrives at the blockage and the velocity begins to decrease. At $t = 10.033$s the wave front has completely passed through the blockage. While the velocity in the blockage has decreased significantly, it is not zero because the Joukowsky pressure generated at the valve is not enough to arrest the flow in the blockage section. This can be explained by recalling that, due to continuity, the steady state velocity in the downstream pipe is smaller than the velocity in the blocked section. Therefore, a valve closure produces just enough pressure to arrest the flow in the downstream pipe, but this pressure cannot completely arrest the faster flow in the blocked section. Note that this nothing but the phenomena of wave transmission and reflection at the pipe-blockage junction explained in terms of velocity. In addition, it is important to note that the vortex at the right-hand side of the blockage is more intense than the steady state case. Such intensification cannot be captured by the one-dimensional models.

3.4 Effect of blockage length

In this section the blockage midpoint is located at 60m from the reservoir, but the length of blockage varies from 0.1m to 10m. The pressure traces at the valve are plotted in Fig. 11. In this case, a first order time integration scheme with $\Delta x = 0.02$ m, $\Delta t = 3\times10^{-5}$s is used. The figure shows that the amplitude of the wave reflection for the 5m blockage is similar to that for the 10m blockage. However, for the 1 m blockage, the magnitude of the reflected pressure is considerably smaller than either the 5 m or 10 m blockages. In addition, the magnitude of the reflected pressure decreases even further for 0.1 m long blockages. In fact, Meniconi, Brunone, & Ferrante (2012) report the same trend that when the blockage length varies from 6.6 m, 3.56 m, 2.7 m, and 0.48 m to 0.06 m, the magnitude of the pressure reflection decreases with the blockage length.

Why is the reflection from the shorter blockage ($l = 1$m) lower than that for a longer blockage ($l = 10$m)? A possible reason for the decreased reflection is due to numerical diffusion. Although the numerical diffusion due to the spatial grid has been minimized by progressive grid refinement until no further numerical smearing is present (as has been done in Mitra & Rouleau, 1985), numerical diffusion due to the time integration and temporal grid has not been fully investigated. Previously Fig. 8 shows that the pressure signal for larger time step ($\Delta t = 3\times10^{-5}$ s) is smoother than that for smaller time steps ($\Delta t = 1\times10^{-6}$ s). In that case, the blockage length is 10m, although the numerical diffusion does not change the typical pressure amplitude, it changes the shape of pressure trace curve to be smoother. For shorter blockage length, the typical pressure amplitude results might be more sensitive to the time step. This is studied as follows.

Firstly, a second-order time integration scheme with smaller time steps is used to minimize the numerical diffusion. The pressure head traces for the short blockage case (l =1m) are plotted in Fig. 12, and the pressure head trace for long blockage case (l =10m) is also plotted for reference. When a first order time integration scheme is used, the peak pressure reflections, corresponding to point C, are smeared for both large time step size $\Delta t = 1\times10^{-5}$ s and small time step size $\Delta t = 3\times10^{-6}$ s. When second order time integration scheme is used, the peak pressure reflection for small time step size $\Delta t = 3\times10^{-6}$ s reaches the reference peak pressure (l =10m), which means the current solution also recovers the one dimensional MOC solution of Wylie et al. (1993) for the short blockage case.

Secondly, if all numerical errors were removed, the results imply that the wave front becomes completely vertical, which is actually impossible to achieve in practice because there is no transient generation mechanism that can close in zero time. Therefore, it may be instructive to know how wave front smearing, whether due to numerical diffusion or non-zero valve closure (discussed later in Fig. 16), changes the wave reflection amplitude for the following two cases: (i) for short blockage ($l = 1$m) using a first order time integration scheme with moderate time step sizes; and (ii) when the typical reflected pressure wave amplitudes are not observed to change for the case of a long blockage ($l = 10$ m).

The pressure along the pipe axis is plotted for different time in Fig. 13 for the case of 1m long blockage and Fig.14 for the case of 10 m long blockage. Not surprisingly, the pressure distributions in both cases are the same before the wave arrives at the blockage. After reflection from the blockage, the reflected pressure peak from the 10m long blockage is larger than that from the 1m long blockage. To explain, the water hammer wave is smeared as it travels towards the blockage (see dashed wave fronts in Fig. 13 and Fig. 14). The thickness of this transient wave front is several meters. When the smoothed gradual wave front arrives at the blockage it induces an equally smooth and gradual transmitted and reflected wave. If

the thickness of the incident wave is larger than the blockage length, which is the case in Fig. 13, the leading edge of the transmitted wave front passes through the short blockage ($l = 1$m) before its maximum pressure at the rear arrives at the blockage. As a result, part of its leading front is reflected back into the blockage and destructively interferes with maximum pressure at the rear side of the blockage. The net result is a reduction in the amplitude of the reflected wave from the blockage towards the valve. When the thickness of the wave incident at the blockage is smaller than the length of the blockage, which is the case for the long blockage ($l = 10$ m), the maximum rear pressure arrives to the right hand side of the blockage before it interacts with the reflected part of the head of the wave from the left end of the blockage. Therefore, the maximum pressure is achieved as can be seen in the results plotted in Fig. 14.

The key concept in the above explanation is the fact that the wave front becomes smeared as it travels through the pipe. What causes this smearing? One possible source of smearing could be turbulent diffusion of the wave front. An estimate of the order of magnitude of this process is obtained by using $\nu_T = 0.027\sqrt{k}\,l_t$, $k = 1.5(IV)^2$, I is the turbulence intensity and l_t is the length scale for turbulence (ADINA Theory and Modeling Guide, 2010). In the current case $V = 1\,\mathrm{m\,s^{-1}}$, $l_t = D = 0.1$m, and $I = 0.05 \sim 0.1$ give $\nu_T = 0.00016 \sim 0.00033\ \mathrm{m^2 s^{-1}}$. The duration of the wave travel from the valve to the blockage is $t = L_1 / a_0 \approx 40/1414 = 0.0283$ s. Therefore, the wave front thickness induced by turbulent diffusion is of the order $\delta = \sqrt{\nu_T L_1 / a_0}$ which ranges from 0.02 m to 0.03 m in this case. This thickness is much smaller than the smearing observed in Fig. 13 and Fig. 14 which are of the order of a few meters. Therefore, the turbulent diffusion contributes little to the wave-front smearing found in the examples studied in this paper.

The second possible source of smearing could be numerical diffusion. A comparison of wave fronts calculated using varying time step sizes and different time integration schemes are plotted in Fig. 15 for a time period shortly after valve closure and a time period shortly before wave reflection. The wave front for small time step size ($\Delta t = 3\times10^{-6}$ s) and second order time integration scheme is much steeper than that predicted for a larger time step size ($\Delta t = 3\times10^{-5}$ s) and using a first order time integration scheme. Therefore, when a smaller time step size and second order time integration scheme is used the effective thickness of the wave front incident on the blockage is smaller, and the maximum rear pressure arrives at the right hand side of the blockage before it interacts with the reflected part of the head of the wave from the left end of the blockage, resulting in full pressure reflection (Fig. 12).

The quasi-two-dimensional model of Zhao & Ghidaoui (2003) uses MOC along the pipe line for a pipe system. MOC is models the linear water hammer wave front well; in fact, the MOC-based solution is free of numerical diffusion when the Courant–Friedrichs–Lewy

(CFL) condition ($a_0 \Delta t / \Delta x = 1$) is satisfied. However, when a pipeline system with several pipes is studied, there are cases for which the grids cannot satisfy the CFL condition for every pipe. Spatial or temporal interpolation is then necessary in the numerical solution and the reflected pressure amplitude might be underestimated due to the numerical diffusion of the wave front.

ADINA, on the other hand, is a computer code for general fluid problems and uses an implicit time integration scheme for numerical stability. However, calculations show that the implicit time integration scheme may also have large numerical diffusion. In the current study, it is necessary to use a second order integration scheme with small time step size ($\Delta t = 3.0 \times 10^{-6}$ s) to eliminate the effects of numerical diffusion from time integration. The required time step is even smaller than the time step needed for accurate MOC solution. For the current case $\Delta x = 0.02$ m, $a_0 = 1414$ m s^{-1}; if the MOC solution is used, the time step is only $\Delta t = 1.414 \times 10^{-5}$ s, somewhat larger than that needed to solve the ADINA model ($\Delta t = 3.0 \times 10^{-6}$ s). Nevertheless, this study demonstrates the ability of ADINA to solve flow cases with complex geometry in spite of the requirement of smaller time step size for the special case of short blockage.

Another possibility for wave front smearing would be due to the finite time needed to execute the valve closure since it is impossible to have an instantaneous valve closure. If the valve closure takes 0.01 s and the wave speed is about 1400 m s^{-1}, this implies that the wave has already traveled 14 m along the pipe before the valve is fully closed. Figure 16 shows the wave front for different valve closure times. The mean velocity at the valve is assumed to linearly decrease from the initial velocity to zero during the closure time. For slow closure, i.e., the mean velocity at the valve is assumed to vary linearly from its initial value to zero in 0.01 s, the thickness of wave front is more than 10 m in length. This effects may account for the results of Meniconi, Brunone, & Ferrante (2012), which show that when the blockage length varies form 6.6 m, 3.56 m, 2.7 m, and 0.48 m to 0.06 m, the pressure reflection decreases with the blockage length. Other possible reason for wave front smearing in the results of Meniconi, Brunone, Ferrante, et al. (2012) is the viscoelastic pipe effect.

4 Conclusion

A reservoir-pipe-valve system with an extended blockage is simulated with the fluids commercial CFD software ADINA. The blockage is modeled as a short pipe length with a smaller diameter; therefore, a system with three pipes in series is studied. The pressure signal produced with ADINA generally agrees with that produced with the classical one-dimensional MOC solution. Moreover, it is shown that ADINA produces solutions of

sufficient accuracy to examine the interactions between transient waves and pipe blockage. Investigation of the water hammer wave front shows that the wave front is smeared during its travel from the valve to the blockage location. In this study the wave front smearing is found to be mainly due to numerical diffusion, although in practice this smearing will exist mainly because valves do not close instantaneously. When an incident wave impinges on a blockage, if the thickness of the wave front is large compared with the blockage length, then the downstream end of the blockage (relative to the incident wave direction) will interact with the wave front and reflect a negative pressure wave towards the incident wave before its maximum pressure arrives at the upstream end of the blockage. This negative wave reflection significantly reduces the amplitude of the incident wave peak pressure. In this case, the blockage behaves as a discrete blockage. However, if the blockage length is large compared with the thickness of the wave front, the incident wave conserves its initial amplitude, and the blockage behaves as extended blockage.

Funding

This research is supported by the Hong Kong Research Grants Council (RGC) under the projects No. T21-602/15-R, No. 25200616 and No. 15201017, as well as by the National Natural Science Foundation of China under project No. 11472074.

Notation

$A =$ pipe cross sectional area (m^2)

$a_0 =$ water hammer wave speed ($m\ s^{-1}$)

$D =$ pipe diameter (m)

$d =$ small pipe diameter where blockage locates (m)

$\boldsymbol{f}^B =$ body force vector ($kg\ m^{-2}s^{-2}$)

$g =$ gravitational acceleration ($m\ s^{-2}$)

$H =$ pressure head (m)

$\mathbf{I} =$ unit tensor (-)

$I =$ relative turbulence intensity (-)

$K =$ bulk modulus of elasticity of fluid (Pa)

$k =$ turbulence kinetic energy (m^2s^{-2})

$L =$ pipe length (m)

$l =$ blockage length (m)

$l_t =$ length scale for turbulence (m)

$Nr =$ number of grids in radial direction (-)

$p =$ pressure (Pa)

$R =$ pipe radius (m)

$\mathsf{R} =$ Reynolds number (-)

$r =$ radial coordinate (m)

$t =$ time (s)

$u^+ =$ velocity in wall coordinate (-)

$\boldsymbol{v} =$ velocity vector (m s^{-1})

$V =$ velocity scale (m s^{-1})

$V_0 =$ steady state mean velocity (m s^{-1})

$x =$ axial coordinate (m)

$y^+ =$ distance from wall in wall coordinate (-)

$\delta =$ thickness of transient wave front (m)

$\lambda =$ coefficient of fluid viscosity (kg $m^{-1}s^{-1}$)

$\rho_m =$ fluid density with the compressibility (kg m^{-3})

$\rho =$ density at zero pressure $p = 0$ Pa (kg m^{-3})

$\boldsymbol{\tau} =$ stress tensor (Pa)

$\mu =$ dynamic viscosity of fluid (kg $m^{-1}s^{-1}$)

$\mu_t =$ dynamic turbulent viscosity (kg $m^{-1}s^{-1}$)

$v_T =$ turbulent viscosity (m^2s^{-1})

References

Adewumi, M. A., Eltohami, E. S., & Ahmed, W. H. (2000). Pressure transients across constrictions. *Journal of Energy Resources Technology, 122*(1), 34-41.

Adewumi, M. A., Eltohami, E. S., & Solaja, A. (2003). Possible detection of multiple blockages using transients. *Journal of Energy Resources Technology, 125*(2), 154-159.

ADINA Theory and Modeling Guide, III, ADINA CFD & FSI, 2010.

Brunone, B., Ferrante, M., & Meniconi, S. (2008). Discussion of "detection of partial blockage in single pipelines" by PK Mohapatra, MH Chaudhry, AA Kassem, and J. Moloo. *Journal of Hydraulic Engineering, 134*(6), 872-874.

Contractor, D. N. (1965). The reflection of waterhammer pressure waves from minor losses. *Journal of Basic Engineering, 87*(2), 445-451.

De Salis, M. H. F., & Oldham, D. J. (1999). Determination of the blockage area function of a finite duct from a single pressure response measurement. *Journal of Sound and Vibration, 221*(1), 180-186.

De Salis, M. H. F., & Oldham, D. J. (2001). The development of a rapid single spectrum method for determining the blockage characteristics of a finite length duct. *Journal of Sound and Vibration, 243*(4), 625-640.

Duan, H. F. (2016). Sensitivity analysis of a transient-based frequency domain method for extended blockage detection in water pipeline systems. *Journal of Water Resources Planning and Management, 142*(4), 04015073.

Duan, H. F., Lee, P. J., Che, T. C., Ghidaoui, M. S., Karney, B. W., & Kolyshkin, A. A. (2017). The Influence of Non-uniform Blockages on Transient Wave Behavior and Blockage Detection in Pressurized Water Pipelines. *Journal of Hydro-environment Research, 17*(2017), 1-7.

Duan, H. F., Lee, P. J., Ghidaoui, M. S., & Tuck, J. (2014). Transient wave-blockage interaction and extended blockage detection in elastic water pipelines. *Journal of fluids and structures, 46*, 2-16.

Duan, H. F., Lee, P. J., Ghidaoui, M. S., & Tung, Y. K. (2012). Extended blockage detection in pipelines by using the system frequency response analysis. *Journal of Water Resources Planning and Management, 138*(1), 55-62.

Duan, H. F., Lee, P. J., Kashima, A., Lu, J. L., Ghidaoui, M. S., & Tung, Y. K. (2013). Extended blockage detection in pipes using the system frequency response: analytical analysis and experimental verification. *Journal of Hydraulic Engineering, 139*(7), 763-771.

Jiang, Y., Chen, H., & Li, J. (1996). Leakage and blockage detection in water network of district heating system. *ASHRAE Transactions, 102*(1), 291-296.

Lee, P. J., Duan, H. F., Ghidaoui, M. S., & Karney, B. W. (2013). Frequency domain analysis of pipe fluid transient behaviour. *Journal of Hydraulic Research, 51*(6), 609-622.

Lee, P. J., Vítkovský, J. P., Lambert, M. F., Simpson, A. R., & Liggett, J. A. (2008). Discrete blockage detection in pipelines using the frequency response diagram: numerical study. *Journal of Hydraulic Engineering, 134*(5), 658-663.

Meniconi, S., Brunone, B., & Ferrante, M. (2011). In-line pipe device checking by short-period analysis of transient tests. *Journal of Hydraulic Engineering, 137*(7), 713-722.

Meniconi, S., Brunone, B., & Ferrante, M. (2012). Water-hammer pressure waves interaction at cross-section changes in series in viscoelastic pipes. *Journal of fluids and structures, 33*, 44-58.

Meniconi, S., Brunone, B., Ferrante, M., & Massari, C. (2011). Small amplitude sharp pressure waves to diagnose pipe systems. *Water Resources Management*, *25*(1), 79-96.

Meniconi, S., Brunone, B., Ferrante, M., & Massari, C. (2012). Transient hydrodynamics of in-line valves in viscoelastic pressurized pipes: long-period analysis. *Experiments in fluids*, *53*(1), 265-275.

Mitra, A. K., & Rouleau, W. T. (1985). Radial and axial variations in transient pressure waves transmitted through liquid transmission lines. *Journal of Fluids Engineering*, *107*(1), 105-111.

Mohapatra, P. K., Chaudhry, M. H., Kassem, A. A., & Moloo, J. (2006). Detection of partial blockage in single pipelines. *Journal of Hydraulic Engineering*, *132*(2), 200-206.

Quarteroni, A. (2001). Modeling the cardiovascular system—A mathematical adventure: Part I. *SIAM News*, *34*(5), 1-3.

Sattar, A. M., Chaudhry, M. H., & Kassem, A. A. (2008). Partial blockage detection in pipelines by frequency response method. *Journal of Hydraulic Engineering*, *134*(1), 76-89.

Street R. L., Watters G. Z., & Vennard J. K. (1996). *Elementary fluid mechanics*, 7th Ed. New York, NY: John Wiley & Sons.

Vardy, A. E., & Hwang, K. L. (1991). A characteristics model of transient friction in pipes. *Journal of Hydraulic Research*, *29*(5), 669-684.

Wang, X. J., Lambert, M. F., & Simpson, A. R. (2005). Detection and location of a partial blockage in a pipeline using damping of fluid transients. *Journal of Water Resources Planning and Management*, *131*(3), 244-249.

Wu, Q., & Fricke, F. (1989). Estimation of blockage dimensions in a duct using measured eigenfrequency shifts. *Journal of Sound and Vibration*, *133*(2), 289-301.

Wylie, E. B., Streeter, V. L., & Suo, L. S. (1993). *Fluid transients in systems*. Englewood Cliffs, New Jersey: Prentice-Hall.

Zhao, M., & Ghidaoui, M. S. (2003). Efficient quasi-two-dimensional model for water hammer problems. *Journal of Hydraulic Engineering*, *129*(12), 1007-1013.

Zhao, M., & Ghidaoui, M. S. (2006). Investigation of turbulence behavior in pipe transient using ak–∈ model. *Journal of Hydraulic Research*, *44*(5), 682-692.

List of figures

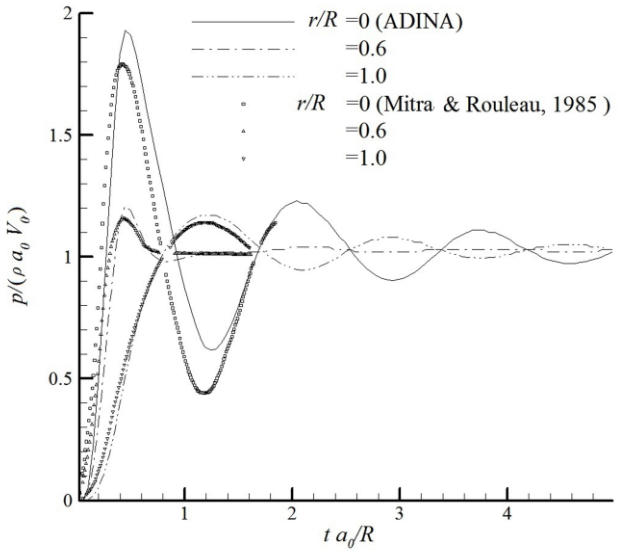

Figure 1 Pressure traces for valve end at different radial locations

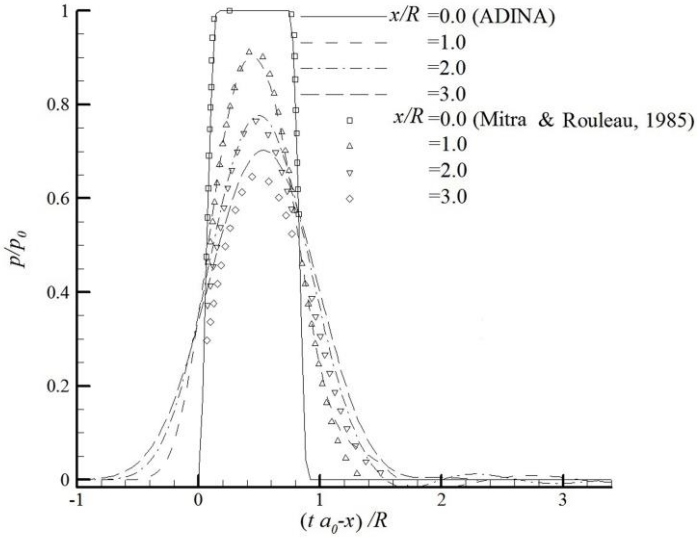

Figure 2 Temporal variations of pressure at several axial stations for the pulse problem

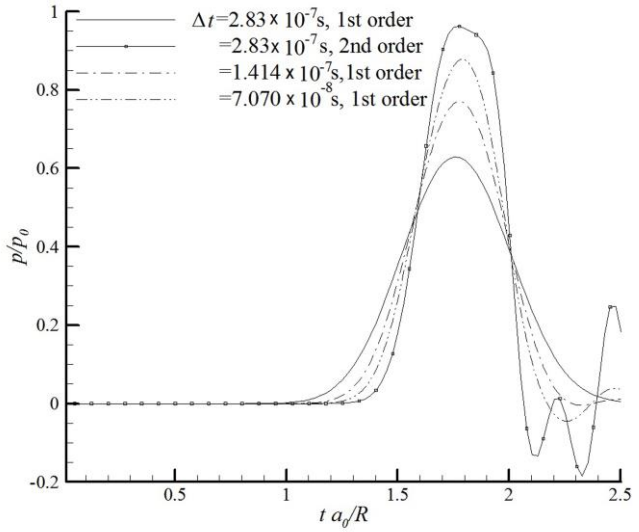

Figure 3 Temporal variations of pressure at $x/R=3$ for different time step sizes and time integration schemes

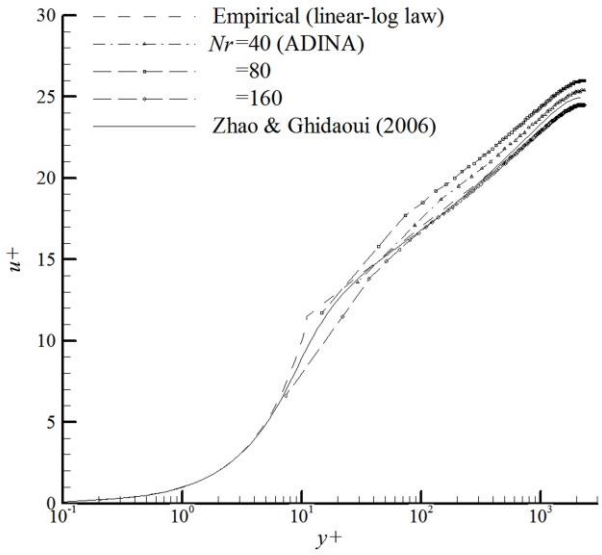

Figure 4 Dimensionless profiles of time-averaged velocity in wall units

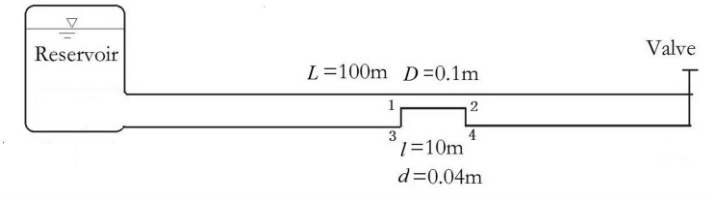

Figure 5 Reservoir-pipe-valve system with an extended blockage (radial direction is scaled by a factor of 100)

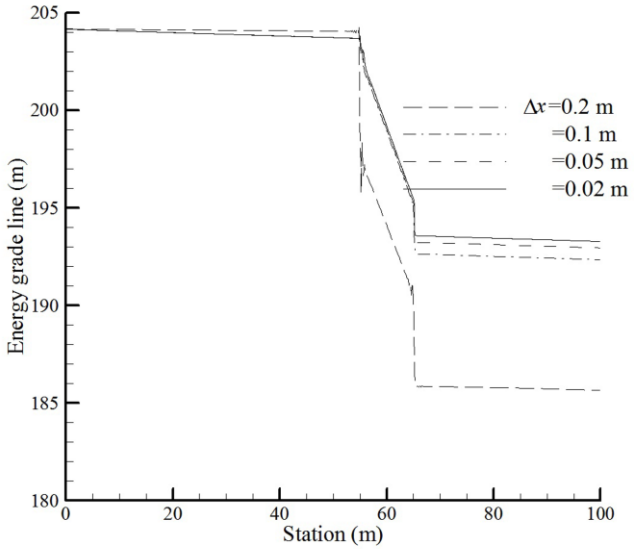

Figure 6 Energy grade lines for the reservoir-pipe-valve system with an extended blockage

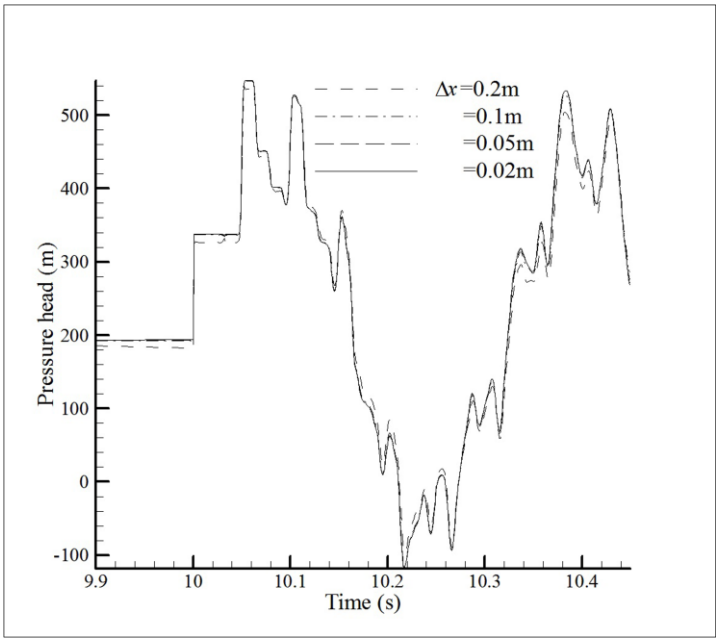

Figure 7 Pressure head traces at the valve end

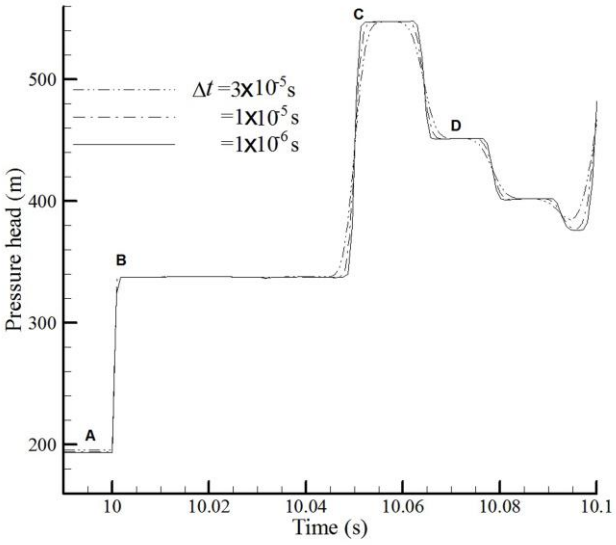

Figure 8 Pressure head traces at the valve end for different time step sizes

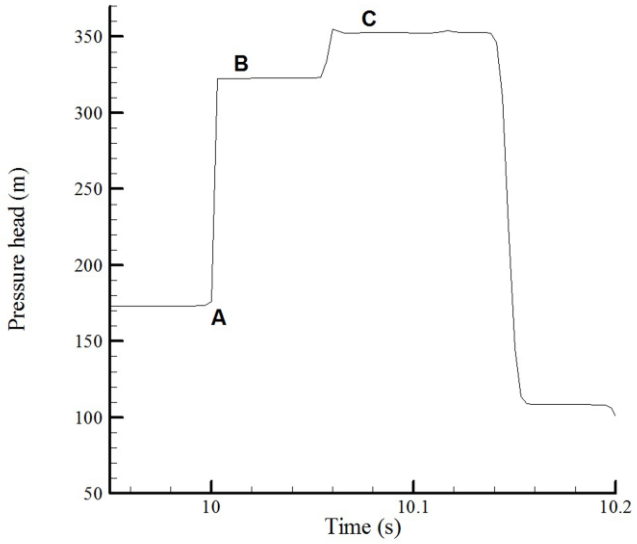

Figure 9 Pressure head traces at the valve end for system with short blockage

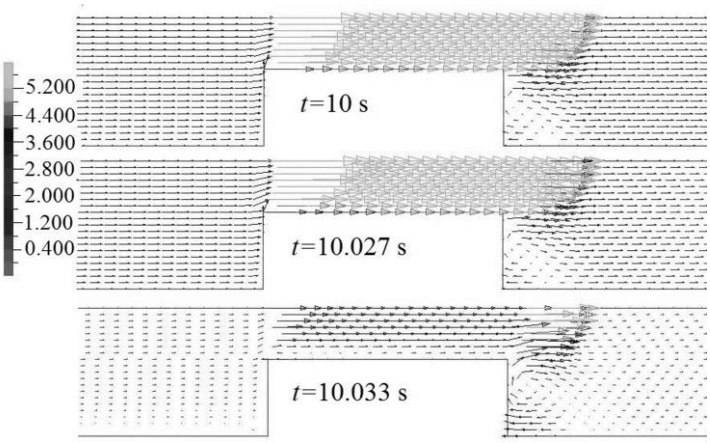

Figure 10 Velocity vectors close to the blockage ($l = 1$m)

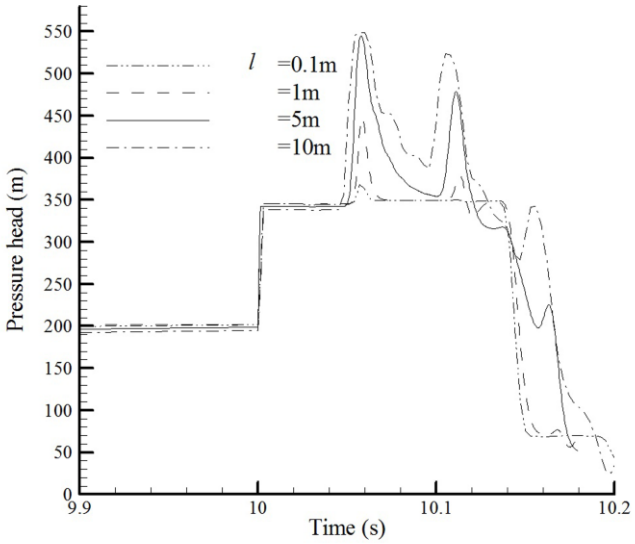

Figure 11 Pressure head traces at the valve end for system with different blockage lengths

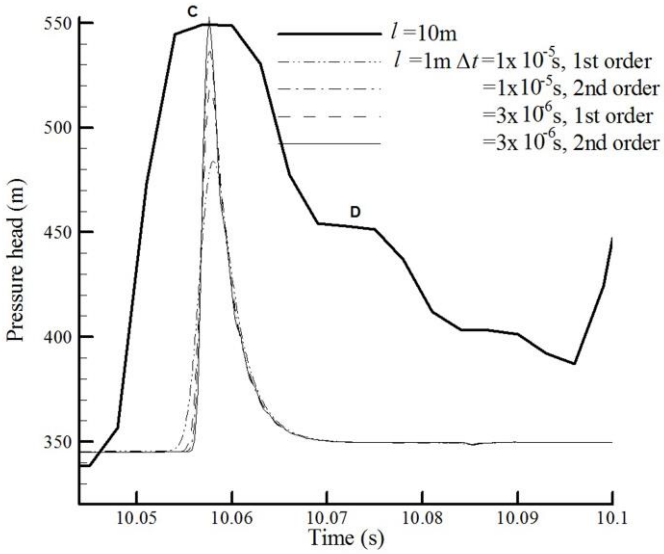

Figure 12 Pressure head traces at the valve end for blockage length $l = 1\text{m}$ with different time step sizes and time integration schemes

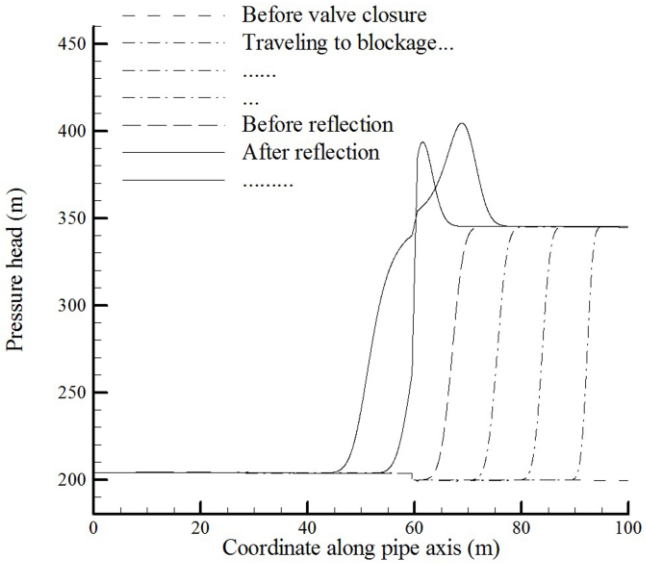

Figure 13 Axial pressure head distribution for 1 m blockage

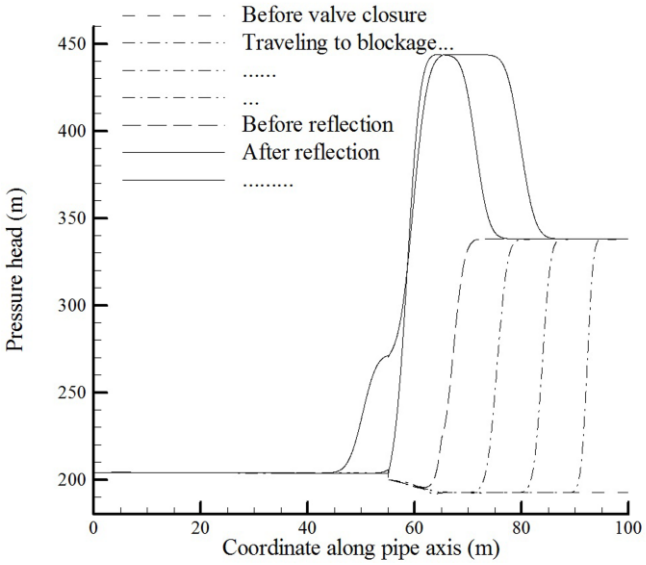

Figure 14 Axial pressure head distribution for 10 m blockage

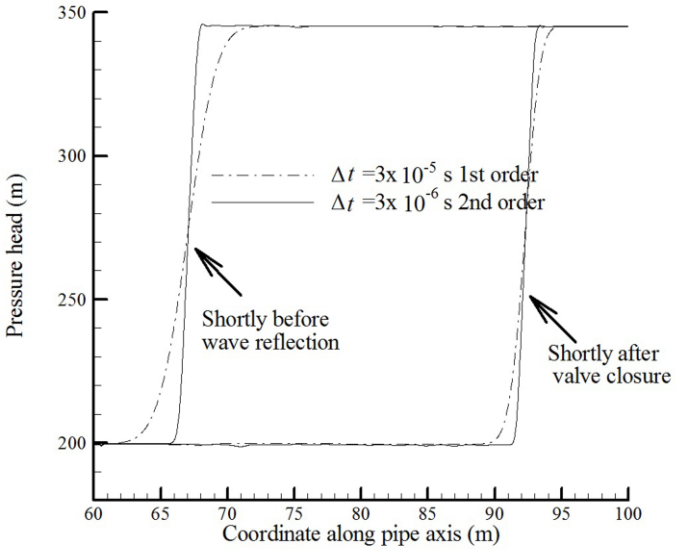

Figure 15 Axial pressure head distribution for 1 m blockage for different time step sizes and time integration scheme

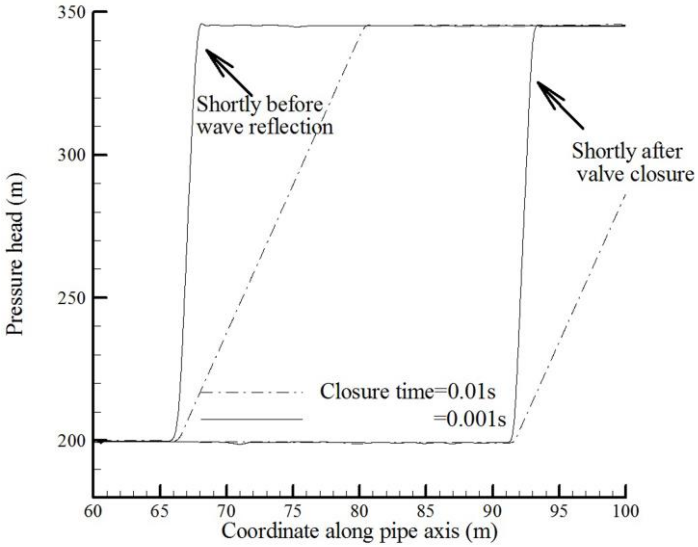

Figure 16 Axial pressure head distribution for 1 m blockage for different valve closure time